The Pcdp1 complex coordinates the activity of dynein isoforms to produce wild-type ciliary motility

Christen G. DiPetrillo and Elizabeth F. Smith
Department of Biological Sciences, Dartmouth College, Hanover, NH 03755

ABSTRACT **Generating the complex waveforms characteristic of beating cilia requires the coordinated activity of multiple dynein isoforms anchored to the axoneme. We previously identified a complex associated with the C1d projection of the central apparatus that includes primary ciliary dyskinesia protein 1 (Pcdp1). Reduced expression of complex members results in severe motility defects, indicating that C1d is essential for wild-type ciliary beating. To define a mechanism for Pcdp1/C1d regulation of motility, we took a functional and structural approach combined with mutants lacking C1d and distinct subsets of dynein arms. Unlike mutants completely lacking the central apparatus, dynein-driven microtubule sliding velocities are wild type in C1d- defective mutants. However, coordination of dynein activity among microtubule doublets is severely disrupted. Remarkably, mutations in either outer or inner dynein arm restore motility to mutants lacking C1d, although waveforms and beat frequency differ depending on which isoform is mutated. These results define a unique role for C1d in coordinating the activity of specific dynein isoforms to control ciliary motility.**

Monitoring Editor
Erika L. F. Holzbaur
University of Pennsylvania

Received: Aug 31, 2011
Revised: Sep 27, 2011
Accepted: Sep 30, 2011

INTRODUCTION

The motility of eukaryotic cilia and flagella requires the precise regulation of dynein-driven microtubule sliding between specific subsets of axonemal doublet microtubules (Satir, 1968, 1985; Summers and Gibbons, 1971, 1973). This regulation must occur along the length of axoneme, circumferentially, and with precise timing. Substantial evidence using a variety of experimental approaches has demonstrated that this regulation involves multiple dynein isoforms, as well as other structures within the axoneme, such as the radial spokes and central apparatus (reviewed in Smith and Yang, 2004; King and Kamiya, 2009; Mitchell, 2009; Wirschell *et al.*, 2009; Yang and Smith, 2009). However, a precise molecular mechanism for how this regulation occurs remains elusive.

In addition to the regulatory cues that control microtubule sliding to generate wild-type motility, certain parameters, such as beat frequency and waveform, may be modulated by intracellular second messengers such as calcium (e.g., Salathe, 2007). As part of an ongoing effort to understand the mechanism of calcium regulation of ciliary motility, we and others have identified several calmodulin (CaM)-interacting complexes anchored to the axoneme (Tash *et al.*, 1988; Yang *et al.*, 2001; Patel-King *et al.*, 2002, 2004; Wargo *et al.*, 2005; Dymek and Smith, 2007; DiPetrillo and Smith, 2010). One of these complexes includes the CaM-binding protein FAP221, which is the *Chlamydomonas* homologue of primary ciliary dyskinesia protein 1 (Pcdp1; Lee *et al.*, 2008), as well as three other proteins (FAP74, FAP46, and FAP54; DiPetrillo and Smith, 2010). Mutants with reduced expression of FAP74 possess flagella that lack most complex components and are missing the C1d projection of the central apparatus (Figure 1A). These artificial microRNA (amiRNA) mutants also have severely impaired motility. Not only is there a significantly reduced percentage of cells that swim, but those cells that are motile have reduced swimming velocity, reduced beat frequency, abnormal waveforms, and defects in calcium-mediated responses, including photoshock and photoaccumulation (DiPetrillo and Smith, 2010). Therefore the FAP221 (Pcdp1) complex is essential for generating wild-type motility in low-calcium conditions, as well as for mediating calcium-induced changes in motility.

Defects in ciliary motility are also observed in Pcdp1-defective mice; these mice have many of the same phenotypes observed in PCD (primary ciliary dyskinesia), including hydrocephalus, respiratory defects (sinusitis), and male infertility (Lee *et al.*, 2008). In

This article was published online ahead of print in MBoC in Press (http://www.molbiolcell.org/cgi/doi/10.1091/mbc.E11-08-0739) on October 12, 2011.

Address correspondence to: Elizabeth F. Smith (elizabeth.f.smith@dartmouth.edu).

Abbreviations used: amiRNA, artificial microRNA; CaM, calmodulin; DHC, dynein heavy chain; WT, wild type.

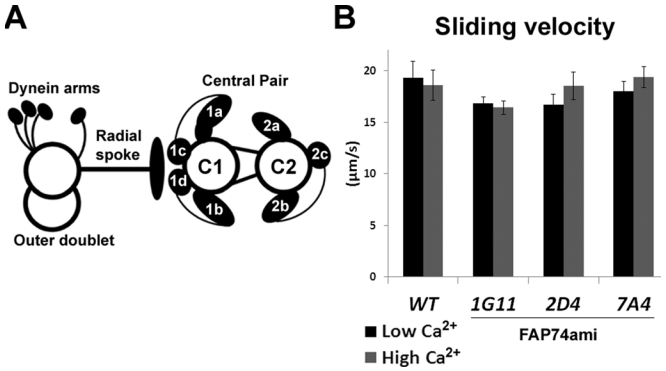

FIGURE 1: Dynein activity is WT in the absence of C1d. (A) Diagram of the central apparatus and a single doublet microtubule with associated structures. Central pair projections are labeled. (B) Microtubule sliding velocities of axonemes isolated from WT and three independent FAP74ami transformants (*1G11*, *2D4*, *7A4*) in low-calcium (black bars) and high-calcium (gray bars) concentrations. Data represent the average of three trials. WT, n = 56; WT + Ca, n = 64; *1G11*, n = 90; *1G11* + Ca, n = 63; *2D4*, n = 76; *2D4* + Ca, n = 44; *7A4*, n = 63; *7A4* + Ca, n = 58. Error bars, ±SEM. Student's *t* test $p > 0.06$ for each FAP74ami strain compared with WT in both low- and high-calcium conditions.

particular genetic backgrounds, homozygous mutant mice die perinatally from hydrocephalus. In other genetic backgrounds, the male mice are infertile, producing sperm with no visible flagella. In these mice, cells of the respiratory tract do produce cilia; however, they beat with reduced frequency and exhibit an abnormal accumulation of mucus in their sinuses. No structural defects were observed in the cilia of these mice.

Given the small structural defect (the lack of the C1d projection) observed in *Chlamydomonas* amiRNA mutants with reduced expression of Pcdp1-complex components, we were surprised that these mutants displayed such severe motility defects. One possibility is that in the absence of the C1d projection, the dynein arms are inactive or incapable of generating efficient sliding between doublet microtubules. A second possibility is that C1d is required for coordinating dynein activity on specific subsets of doublets. To generate effective ciliary and flagellar waveforms, a subset of dynein arms must be active and a subset inactive at any given time during beating. In C1d-defective mutants, the dynein arms may be fully functional but misregulated spatially, temporally, or both such that switching between active and inactive states is not coordinated. These two possibilities are not mutually exclusive, and in either case, subsets of inner and/or outer dynein arm isoforms may be targets for regulation.

To distinguish among these possibilities, we used a combination of functional and structural studies to analyze mutants lacking C1d, and for some experiments also lacking distinct subsets of dynein arms. To determine whether dynein-driven microtubule sliding is wild type (WT), we used an in vitro sliding assay (Summers and Gibbons, 1971; Okagaki and Kamiya, 1986). This assay uncouples dynein-driven microtubule sliding from ciliary bending and allows for quantification of dynein activity in motility-defective mutants by measuring the velocity of microtubule sliding. For example, mutants that lack the entire central apparatus or radial spokes have decreased sliding velocities compared with WT, indicating that dynein activity is reduced in the absence of these structures (Smith and Sale, 1992; Smith, 2002b). If the C1d projection is required for WT dynein activity, we would predict that C1d-defective mutants have reduced microtubule sliding velocities.

To experimentally determine whether microtubule sliding is misregulated spatially or temporally is significantly more challenging. Numerous studies have led to a model in which specific central pair projections make physical contact with the radial spokes on subsets of doublets to locally control dynein-driven microtubule sliding (reviewed in Smith and Yang, 2004). In *Chlamydomonas*, the central apparatus rotates with a slight twist, thus potentially providing structural cues both circumferentially and along the length of the axoneme (Omoto *et al.*, 1999). Unregulated microtubule sliding in C1d-defective mutants may result from a failure of the central apparatus to maintain proper orientation to locally control dynein-driven microtubule sliding. Alternatively, the central pair may rotate in C1d-defective mutants but not provide the necessary structural cues for localized control of sliding.

To determine the orientation of the central apparatus with respect to regions of active sliding, as well as to identify which subsets of doublet microtubules actively slide, we and others have taken a combined structural and functional approach. Using the same in vitro microtubule sliding assay described earlier, we immediately fixed axonemes for subsequent transmission electron microscopy (Yoshimura and Shingyoji, 1999; Nakano *et al.*, 2003; Wargo and Smith, 2003; Wargo *et al.*, 2004). By examining transverse sections of slid *Chlamydomonas* axonemes, we demonstrated that the C1 central microtubule maintains a specific orientation relative to the doublets undergoing active sliding, suggesting a relationship between specific structures on the C1 microtubule and active dynein-driven microtubule sliding (Wargo and Smith, 2003). Furthermore, in both *Chlamydomonas* and sea urchin sperm axonemes specific subsets of doublets undergo sliding in low- versus high-calcium buffer conditions (Nakano *et al.*, 2003; Wargo *et al.*, 2004), and this specificity is disrupted in *Chlamydomonas* mutants lacking specific axonemal structures (Wargo *et al.*, 2004). Following this line of research, we used the same approach in this study to determine whether the orientation of the central apparatus is disrupted in C1d-defective mutants and to assess whether the same subsets of doublet microtubules undergo active sliding in mutant axonemes as they do in wild type. Here, we report that mutants lacking the C1d projection of the central apparatus generate WT dynein-driven microtubule sliding velocities. However, microtubule sliding patterns are disrupted, indicating that dynein-driven microtubule sliding is spatially misregulated despite the presence of fully functional dynein arms. In addition, we discovered that second mutations in dynein arms restore motility to mutants lacking C1d and that C1d appears to differentially regulate the activity of outer and inner dynein arm isoforms. Taken together, these findings support a fundamental and unique role for C1d in regulating specific dynein isoforms and control of ciliary motility.

RESULTS

Coordination of microtubule sliding between specific doublets is disrupted in the absence of C1d

To quantify dynein activity in C1d-defective mutants, we performed an in vitro microtubule sliding assay using three independent FAP74-amiRNA transformants (*1G11, 2D4, 7A4*) that have reduced FAP74 levels and lack the C1d projection of the C1 central tubule (DiPetrillo and Smith, 2010). If reduced dynein activity is the sole cause of the motility defects seen in FAP74ami mutants, we hypothesized that microtubule sliding velocities would be decreased compared with WT, similar to other central pairless mutants (Smith, 2002b). To our surprise, sliding velocities of all three amiRNA mutants were not significantly different from that of WT in either low- or high-calcium concentrations ($p > 0.06$, Student's *t* test; Figure 1B). The expression

A

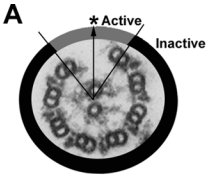

		P8	P7	P6	P5	P4	P3	Total	%
Observed	Active	13	21	17	15	12	7	85	72.65
	Inactive	16	8	4	2	2	0	32	27.35
	Total	29	29	21	17	14	7	117	100
Active Fraction		2/9	3/9	4/9	5/9	6/9	7/9		
Inactive Fraction		7/9	6/9	5/9	4/9	3/9	2/9		
								Total	%
Expected	Active	6.44	9.67	9.33	9.44	9.33	5.44	49.67	42.45
	Inactive	22.56	19.33	11.67	7.56	4.67	1.56	67.33	57.55
	Total	29	29	21	17	14	7	117	100

B

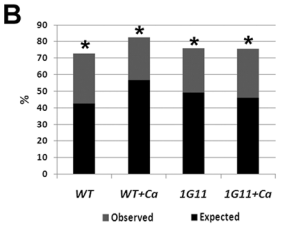

C

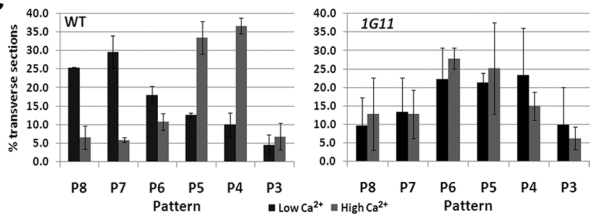

FIGURE 2: C1d is not required for central pair orientation and yet is required for normal microtubule sliding patterns. (A) Top left, electron micrograph of an axoneme transverse section after microtubule sliding. The arrow defines the orientation of the C1 central microtubule. The point at which the arrow intersects the circumference of the outer doublets is indicated by an asterisk. The area of active microtubule sliding is shaded gray. The inactive area is shaded black. The table is a quantitative analysis of central apparatus orientation with diagrams of the six possible patterns produced by active microtubule sliding shown above. Only transverse sections in which the central apparatus remains attached were analyzed. For simplicity, the central apparatus is not shown in the cartoons. The example shown is wild-type axonemes in the low-calcium condition. After recording the observed number of events, we calculated the expected number of events for both the active and inactive areas for each pattern of microtubule sliding if the orientation of the central apparatus was random. Expected events = (fraction of the axoneme in the active or inactive area) × (total events for sliding pattern). The expected events in the active and inactive areas were summed for all sliding patterns (Total), expressed as a percentage of the total number of transverse sections (%), and compared with the percentage of observed events. For further explanation, see *Materials and Methods*. (B) Percentage of transverse sections in which the C1 microtubule is orientated toward the active area of sliding in either low calcium (WT and *1G11*) or high calcium (WT + Ca and *1G11* + Ca) concentrations. The black bars indicate the expected percentage of events (see description in A or *Materials and Methods*). The difference between the observed and expected percentages is shaded in gray. Asterisks denote strains in which the difference between observed and expected percentages is significant (χ^2 test, $p < 0.01$). Data are a combination of two trials. WT, n = 117; WT + Ca, n = 89; *1G11*, n = 116; *1G11* + Ca, n = 94. (C) Distributions of the microtubule sliding patterns following microtubule sliding in low calcium (black bars) or high calcium (gray bars) concentrations. Data represent the average of two trials. WT, n = 142; WT + Ca, n = 104; *1G11*, n = 125; *1G11* + Ca, n = 107.

of FAP74 is most reduced in strain *1G11* (DiPetrillo and Smith, 2010); therefore we focused our experiments on this strain for all further analyses.

Because dynein-driven microtubule sliding velocities are WT in the absence of C1d, the gross motility defects in FAP74ami transformants must be caused by failed coordination of dynein arm activity among the microtubule doublets. We previously reported that in the sliding assay, the central apparatus is normally oriented toward the region of active microtubule sliding (Wargo and Smith, 2003). Based on structural studies of beating *Chlamydomonas* flagella by Mitchell (2003), this central pair orientation in the in vitro sliding assay corresponds to the principal bend of the effective stroke. It is possible that in the absence of C1d, the central apparatus fails to make proper associations with the spoke heads such that active sliding occurs randomly with respect to central pair orientation.

To determine whether the C1 microtubule is preferentially oriented toward the area of active microtubule sliding in C1d-defective mutants, we performed the in vitro microtubule sliding assay using axonemes isolated from FAP74 amiRNA mutants in both low- and high-calcium conditions that were immediately fixed for electron microscopy. For our analysis we only include slid axonemes in which the central apparatus remains associated with the doublets. As shown in Figure 2, slid axonemes viewed in transverse section may appear as one of six different sliding patterns with respect to the number of doublets that remain associated with the central apparatus (central apparatus is not included in diagrams, for simplicity). For each pattern we calculated the percentage of cross sections in which we observed C1 oriented toward the active area of sliding (Figure 2A). We then calculated the percentage of cross sections in which we expected to find C1 oriented toward the active area of sliding if the orientation of the central pair was random (Figure 2A) and used the χ^2 test to determine whether these two percentages are significantly different (see *Materials and Methods*). We found that in the *1G11* mutant, the orientation of the C1 microtubule is not random; rather, C1 is preferentially oriented toward the area of active microtubule sliding in both low- and high-calcium conditions (Figure 2B). These results demonstrate that C1d is most likely not necessary for proper central apparatus orientation.

If dynein activity is WT and the central apparatus is properly oriented in C1d-defective mutants, defective motility is likely due to unregulated dynein activity among the doublet microtubules. To determine whether C1d is involved in spatial coordination of microtubule sliding on specific subsets of doublet microtubules, we analyzed the pattern of microtubule sliding for transverse sections of slid axonemes. Pattern is defined as the number of doublets that remain associated with the central pair after sliding (Figure 2A; also see Wargo *et al.*, 2004). In low-calcium buffer, WT axonemes predominantly slide with the P7 and P8 patterns, whereas in high-calcium conditions the P4 and P5 patterns are most prevalent (Figure 2C; also see Wargo *et al.*, 2004). Of interest, we found in both low- and high-calcium conditions that slid axonemes from *1G11* generate an intermediate sliding pattern (P4–P6) that is more similar to the WT high calcium–induced pattern (Figure 2C). These results support the hypothesis that in the absence of C1d, coordination of dynein-driven microtubule sliding is not WT. To determine more precisely which doublets actively slide in this assay, we used structural markers defined by Hoops and Witman (1983) to identify

the doublet on the dynein exposed edge in transverse section. Although it is difficult to find transverse sections of slid axonemes in which doublet number can be unequivocally determined, doublet numbers 1 and 2 were predominately found on the dynein exposed edge for both WT and *1G11* axonemes (Supplemental Figure S1), as we previously reported for WT axonemes (Wargo *et al.*, 2004). As we reported (Wargo *et al.*, 2004), in the predominately P7–P8 pattern found in WT axonemes in low-calcium buffer, in which doublets 3 (Db3) and Db4 are absent, the doublets with active dynein arms are Db2, Db3, and/or Db4. In a predominately P5 sliding pattern with Db2 prevalent on the dynein exposed edge, doublets with active dynein arms may include any of those on Db2–6.

Subsets of dynein isoforms are differentially affected in C1d-defective mutants

Our data implicate C1d in coordinating dynein activity among the doublet microtubules. To determine whether this coordination differentially affects specific dynein arm isoforms, we constructed double mutants lacking C1d and distinct subsets of dynein arms. Double mutants were generated using *1G11* or *2D4* and the well-characterized *Chlamydomonas* dynein mutants *pf28*, *ida1*, and *ida5*. The *pf28* mutant fails to assemble the outer dynein arms due to a mutation in the γ-dynein heavy chain (DHC) gene (Mitchell and Rosenbaum, 1985; Kamiya, 1988; Wilkerson *et al.*, 1994). The *ida1* mutant lacks inner dynein arm f (also known as I1) due to a mutation in the 1α DHC1 gene; the inner dynein arm f isoform has been strongly implicated in regulating microtubule sliding and ciliary motility (Kamiya *et al.*, 1991; Smith and Sale, 1991; Porter *et al.*, 1992; Habermacher and Sale, 1997; King and Dutcher, 1997; Myster *et al.*, 1997; Hendrickson *et al.*, 2004; Wirschell *et al.*, 2007). The *ida5* mutant was chosen because it lacks four of the six single-headed inner dynein arms (inner dynein arms a and c–e) due to a mutation in the actin gene (Kato *et al.*, 1993; Kato-Minoura *et al.*, 1997). Western blots of axonemes isolated from WT, *1G11*, *pf28*, *ida1*, *ida5*, and the corresponding double mutants were performed to confirm mutant identity (Figure 3, A and B).

We predicted that if any of the dynein isoforms lacking in the double mutants are the target of regulation by the C1d projection, then the double mutants should not have additional motility defects. If the dynein isoforms are not in the same regulatory pathway as C1d, then we predicted the double mutants would have more severe motility defects, such as complete paralysis. Of importance, for all motility data presented later the same results were obtained for *1G11* and *2D4* double mutants. For simplicity, we only included the data for *1G11* and *1G11* double mutants in subsequent figures.

Remarkably, we discovered that the percentage of motile cells dramatically increased in populations of *1G11xpf28* and *1G11xida1*, but not *1G11xida5*, compared with *1G11* (Figure 3C). As previously reported, 31% of *1G11* mutants are able to progressively swim forward (Figure 3C; DiPetrillo and Smith, 2010). Of the remaining two-thirds of the population, approximately half modestly twitch and/or spin in place, and half are paralyzed or stuck to the microscope slide (data not shown). In contrast, <4% of WT, *pf28*, *ida1*, *ida5*, *1G11xida1*, or *1G11xpf28* cells are twitchy (data not shown). The remaining small percentage of cells not accounted for in the swimming population (Figure 3C) are paralyzed or stuck to the microscope slide (data not shown). Although the percentage of swimming cells did not significantly increase in *1G11xida5,* the swimming population showed more wild-type motility, as described later.

To characterize motility in the swimming population of double mutants, we used high-speed video analysis. The mean swimming

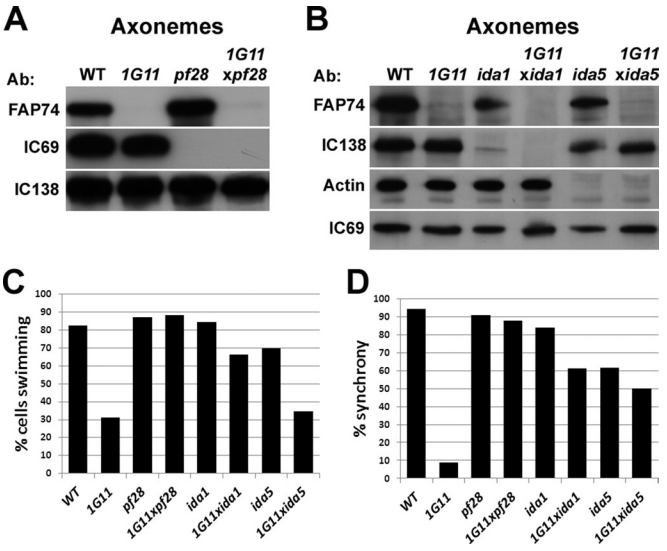

FIGURE 3: Double mutants have recovered swimming populations and flagellar synchrony. (A, B) Western blots of axonemes isolated from WT and mutants cells. FAP74 is a member of the C1d complex (lacking from *1G11*) and IC69 is an intermediate chain of the outer dynein arms (Mitchell and Kang, 1991) (lacking from *pf28*). IC138 is an intermediate chain of the inner dynein arm f (Porter *et al.*, 1992; Hendrickson *et al.*, 2004) (lacking from *ida1*). Actin is a light chain of a subset of inner dynein arms (Piperno and Luck, 1979; Kato-Minoura *et al.*, 1997) and is required for inner dynein arms a and c–e assembly (lacking in *ida5*). FAP74 and IC69 are lacking from *1G11xpf28*, FAP74 and IC138 are lacking from *1G11xida1*, and FAP74 and actin are lacking from *1G11xida5*, confirming the identities of double mutants. (C) Percentage of cells in WT and mutant populations that swim forward. Cells with twitchy flagella that only jiggle in place are not included in this percentage. WT, n = 281; *1G11*, n = 299; *pf28*, n = 246; *1G11xpf28*, n = 418; *ida1*, n = 304; *1G11xida1*, n = 290; *ida5*, n = 433; *1G11xida5*, n = 265. (D) Percentage of beat cycles in which the flagella are in synch. Percentages are calculated from the total number of beats scored for each strain: WT, n = 398 beats; *1G11*, n = 275; *pf28*, n = 427; *1G11xpf28*, n = 344; *ida1*, n = 324; *1G11xida1*, n = 298; *ida5*, n = 251; *1G11xida5*, n = 241.

velocities of *1G11* (33.2 μm/s) and *1G11xpf28* (29.8 μm/s) are not significantly different from each other, but they are significantly lower than those of *pf28* (50.0 μm/s) (Figure 4A). Three parameters that contribute to forward swimming velocity are ciliary beat frequency, waveform, and synchrony between flagella. The mean beat frequencies of *1G11* (15.0 Hz) and *1G11xpf28* (14.4 Hz) are not significantly different from each other, but they are significantly lower than that of *pf28* (22.8 Hz) (Figure 4B). Remarkably, the two flagella of *1G11xpf28* no longer beat asynchronously as is observed in *1G11* (Figure 3D). In addition, the flagellar waveform of *1G11xpf28* is qualitatively more similar to that of WT and *pf28* than that of *1G11* (Figure 4G and Supplemental Videos S1–S4). Therefore the restoration in motility in *1G11* in the absence of outer dynein arms is not due to changes in beat frequency but rather to restoration of synchrony between the two flagella, as well as to the effective propagation of bends and conversion to a more WT waveform. Note that the small percentage of asynchronous beats in WT cells agrees with the work of Ruffer and Nultsch (1998).

Restoration of motility in double mutants lacking inner dynein arm isoforms quantitatively and qualitatively differs from that restored by outer dynein arm mutations. The swimming velocity of *1G11xida1* (45.6 μm/s) is significantly higher than that of *1G11*

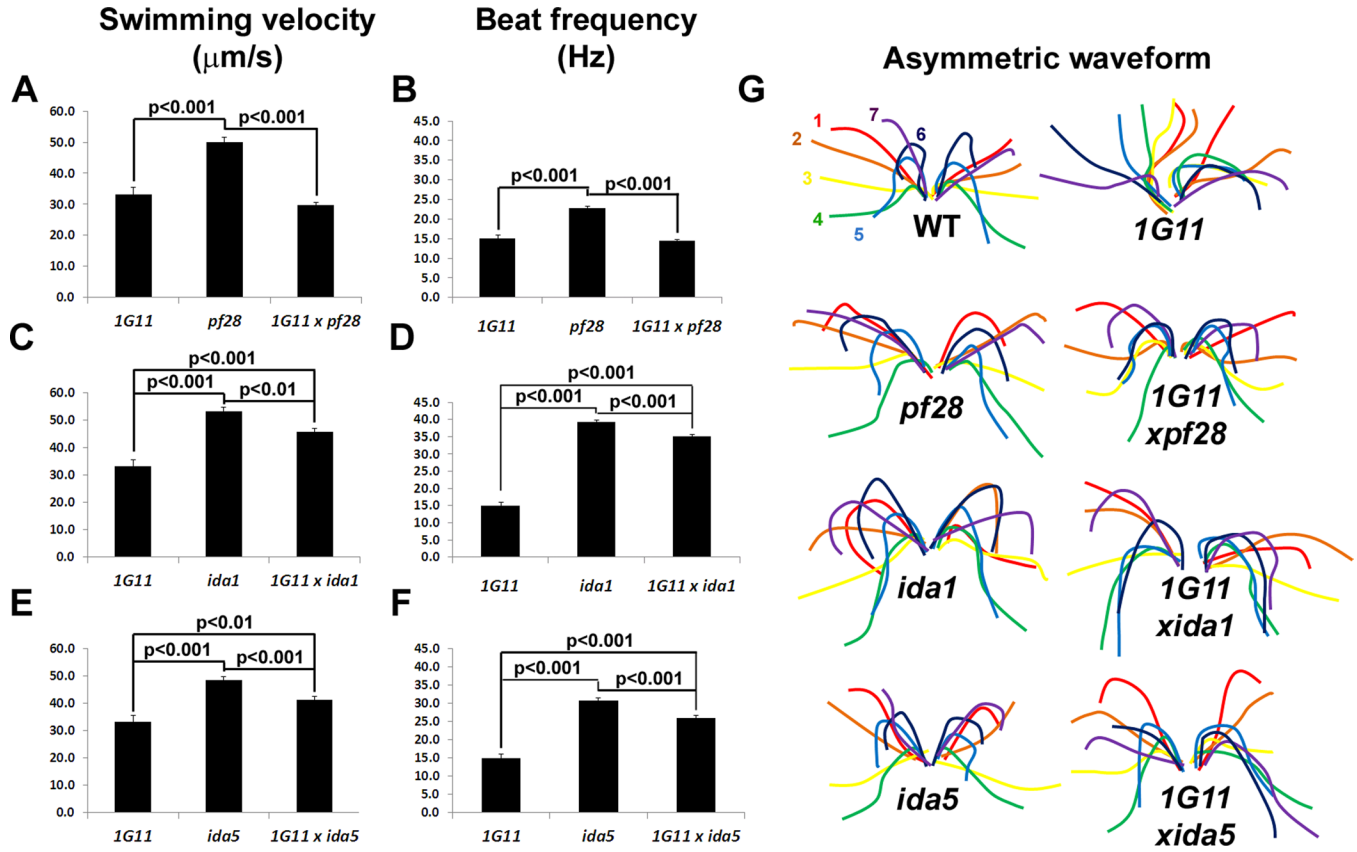

FIGURE 4: Inner dynein arm double mutants have recovered motility parameters. Mean swimming velocities (A, C, E) and mean beat frequencies (B, D, F) of *1G11* compared with *pf28* and *1G11xpf28* (A, B), *ida1* and *1G11xida1* (C, D), and *ida5* and *1G11xida5* (E, F). Black lines connect values with significant differences (determined by Student's *t* test); p values are noted. For swimming velocities: *1G11*, n = 89; *pf28*, n = 92; *1G11xpf28*, n = 79; *ida1*, n = 81; *1G11xida1*, n = 93; *ida5*, n = 87; *1G11xida5*, n = 94. For beat frequencies: *1G11*, n = 99; *pf28*, n = 172; *1G11xpf28*, n = 177; *ida1*, n = 165; *1G11xida1*, n = 145; *ida5*, n = 170; *1G11xida5*, n = 172. (G) Diagrams showing the progression of the asymmetric waveform of a representative cell from WT and each mutant strain as traced from a recorded video (see *Materials and Methods*). Numbers and colors represent the order of each flagellar position over time. The time between each flagellar position (color) is 0.004 s (WT), 0.006 s (*ida1*, *1G11xida1*, *ida5*, and *1G11xida5*), or 0.008 s (*1G11*, *pf28*, and *1G11xpf28*).

(33.2 μm/s), although it is significantly lower than that of *ida1* (53.0 μm/s; Figure 4C). This result suggests that the loss of inner dynein arm f relieves the dynein inhibition responsible for the decreased swimming velocity of *1G11*. Remarkably, a similar result is found with the *ida5* double mutant. Despite having a small percentage of motile cells, similar to *1G11* (Figure 3C), the swimming velocity of *1G11xida5* (41.1 μm/s) is significantly increased compared with that of 1G11 (33.2 μm/s; Figure 4E), although it is significantly lower than that of *ida5* (48.3 μm/s; Figure 4E). The increased swimming velocity observed for *1G11xida1* and *1G11xida5* is due in large part to increased beat frequencies (Figure 4D,F). In addition, for both *1G11xida1* and *1G11xida5* synchrony between the two flagella was restored (Figure 3D). Although some asymmetries in waveform between the two flagella of *1G11xida1* and *1G11xida5* were observed and waveforms were not entirely WT, they were substantially recovered compared with *1G11* (Figure 4G; Supplemental Videos S5–S8).

As indicated by recovered motility and suggested by the waveform traces shown in Figure 4G, *1G11*:dynein double mutants have significantly restored waveforms compared with the *1G11* mutant alone. To quantify changes in waveform, we measured the radius of curvature for the principal bend of the recovery stroke (the most obvious bend) for all strains (Supplemental Figure S2). The radius of curvature for *1G11* is significantly larger than that for wild type ($p < 0.001$). Yet, in all double-mutant strains, the radius of curvature was not significantly different from that of the corresponding single dynein mutant. Therefore the absence of specific dynein arm subforms restores the ability of strain *1G11* to generate effective bends.

Because the C1d complex binds to calmodulin in a calcium-dependent manner, we hypothesized C1d may play a role in calcium-induced changes of dynein regulation. Two calcium-modulated behaviors in *Chlamydomonas* are photoshock and phototaxis (Hyams and Borisy, 1978; Bessen *et al.*, 1980; Kamiya and Witman, 1984; Witman, 1993). We previously reported that *1G11* is defective in the photoshock response (DiPetrillo and Smith, 2010). Only a small percentage of cells switch to the symmetric waveform upon exposure to bright light. Given the significantly restored motility of *1G11* double mutants, we tested whether the conversion to a symmetric waveform was also restored. All mutant cells have a decreased percentage of cells capable of converting to the symmetric waveform compared with WT (Figure 5A). For the small percentage of cells able to switch waveforms, we calculated the symmetric beat frequencies. Although the symmetric beat frequency of *pf28* is

A

Cell type	Structural defect	Photo-accumulation	% Photoshock (n)	Symmetric beat frequency (Hz ± SEM)
WT	None	++	100 (91)	76.0 ± 3.0
1G11	C1d	-	4 (91)	58.9 ± 4.5
pf28	ODA	+	22 (76)	44.7 ± 3.0
1G11xpf28	C1d, ODA	-	11 (98)	23 ± 1.7
ida1	IDA f	-	10 (88)	67.3 ± 5.5
1G11xida1	C1d, IDAf	-	0 (91)	ND
ida5	IDA a,c,d,e	+	1 (101)	25.9 (n=1)
1G11xida5	C1d, IDA a,c,d,e	-	0 (97)	ND

B

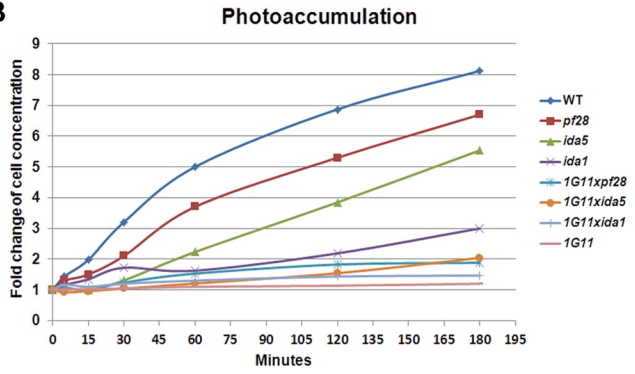

FIGURE 5: Calcium-mediated motility phenotypes of single and double dynein mutants. (A) Table listing each cell strain used in this study along with the associated structural defect, ability to photoaccumulate (which is quantified in B), percentage of cells able to convert to the symmetric waveform, and the average symmetric beat frequency for those cells that are able to photoshock. (B) The fold change in the concentration of cells at the light-exposed edge of the Petri dish used in the photoaccumulation assay. Time points were taken at 0, 5, 15, 30, 60, 120, and 180 min, and the fold change compared with the 0-min time point was plotted. See *Materials and Methods* for details of quantification.

decreased compared with that of *1G11*, the beat frequency of *1G11xpf28* is dramatically and significantly reduced compared with that of both parental strains. The symmetric beat frequencies of *1G11* and *ida1* are modestly decreased compared with WT; however, *1G11xida1* is incapable of converting to the symmetric waveform. Both *ida5* and *1G11xida5* fail to convert to the symmetric waveform. For the one observed *ida5* cell that displayed a weak symmetric waveform, the beat frequency is severely reduced compared with *1G11* and WT (Figure 5A).

To analyze the ability of mutant cells to phototax, we used a simple photoaccumulation assay (see *Materials and Methods*). *Chlamydomonas* mutants are typically considered phototaxis defective if photoaccumulation does not occur within 10 min (King and Dutcher, 1997). We previously reported that *1G11* took many hours to photoaccumulate. However, it was not clear whether this defect was due to the severe motility defects in this mutant. Therefore we tested the ability of the motile single- and double-mutant strains for recovery of efficient photoaccumulation (Figure 5). As previously reported, *ida1* is defective for photoaccumulation, and *pf28* can positively phototax, albeit more slowly than wild type (Mitchell and Rosenbaum, 1985; Horst and Witman, 1993; King and Dutcher, 1997; Okita *et al*., 2005). The *ida5* mutant alone is also able to photoaccumulate, although this occurs more slowly than for either WT or *pf28*.

All analyzed double mutants eventually accumulate at the illuminated edge of the Petri dish, although it still took many hours for photoaccumulation to occur. Data illustrating this delay are shown graphically in Figure 5B. Considering that the length of the Petri dish in which we assess photoaccumulation is 100 mm, even for the slowest mutant, *1G11xpf28,* which swims at 29.8 μm/s, photoaccumulation should take at most 1 h. The low swimming velocities alone cannot explain why all the mutants tested take substantially longer than 1 h to photoaccumulate, often taking >12 h. Therefore we consider all analyzed double mutants to have photoaccumulation defects.

Analysis of in vitro microtubule sliding for dynein- and C1d-defective double mutants

To quantify dynein activity in double-mutant axonemes, we performed the microtubule sliding assay. Sliding velocities are wild type in *1G11* (Figure 1B); however, the presence of the outer dynein arms may mask more subtle changes in dynein activity of inner dynein arm isoforms. The outer dynein arms are known to be the major power source in axonemal sliding. Predictably, sliding velocities in *1G11xpf28* axonemes are significantly reduced compared with those in *1G11* regardless of calcium concentration (Figure 6A). However, since *1G11xpf28* sliding velocities are not significantly different from those in *pf28*, it appears that the inner dynein arm activity is normal in this double mutant. Sliding velocities of *1G11* are not significantly different from those of either *1G11xida1* or *ida1* in low- or high-calcium buffer (Figure 6B). The sliding velocity of *1G11xida5* is only slightly, yet significantly, decreased compared with that of *1G11* in both calcium conditions (Figure 6C). *1G11xida5* sliding velocity is significantly decreased compared with that of *ida5* in high- but not low-calcium concentrations (Figure 6C). However, no significant difference is observed between *ida5* and *1G11* in either the low- or high-calcium condition (Figure 6C). On the basis of these combined results, the lack of the C1d projection does not substantially affect the ability of specific dynein isoforms to generate effective sliding between doublet microtubules.

That the *1G11* double mutants can swim implies that the defect in coordinating microtubule sliding among the doublet microtubules in *1G11* is suppressed by the absence of specific dynein arms. Therefore we predicted that this suppression would result in an observable change in microtubule

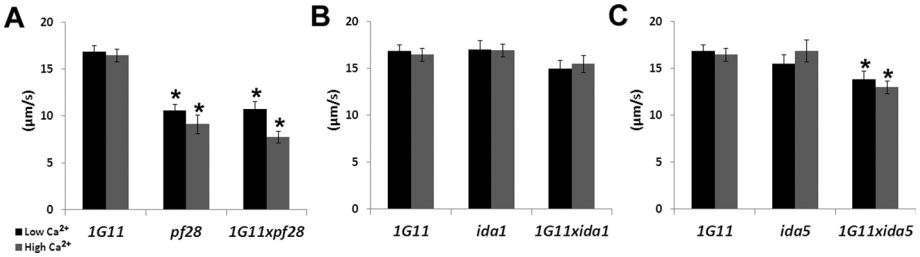

FIGURE 6: Dynein-driven microtubule sliding velocity is relatively normal in double mutants. Average microtubule sliding velocities in low calcium (black bars) and high calcium (gray bars) concentrations of *1G11* compared with (A) *pf28* and *1G11xpf28*, (B) *ida1* and *1G11xida1*, and (C) *ida5 and 1G11xida5*. Asterisks represent a significant difference from *1G11*, Student's *t* test, $p < 0.01$. Data represents the average of three trials. *1G11*, n = 90; *1G11* + Ca, n = 63; *pf28*, n = 66; *pf28* + Ca, n = 23; *1G11xpf28*, n = 40; *1G11xpf28* + Ca, n = 41; *ida1*, n = 66; *ida1* + Ca, n = 70; *1G11xida1*, n = 57; *1G11xida1* + Ca, n = 56; *ida5*, n = 54; *ida5* + Ca, n = 56; *1G11xida5*, n = 62; *1G11xida5* + Ca, n = 65. Error bars, ±SEM.

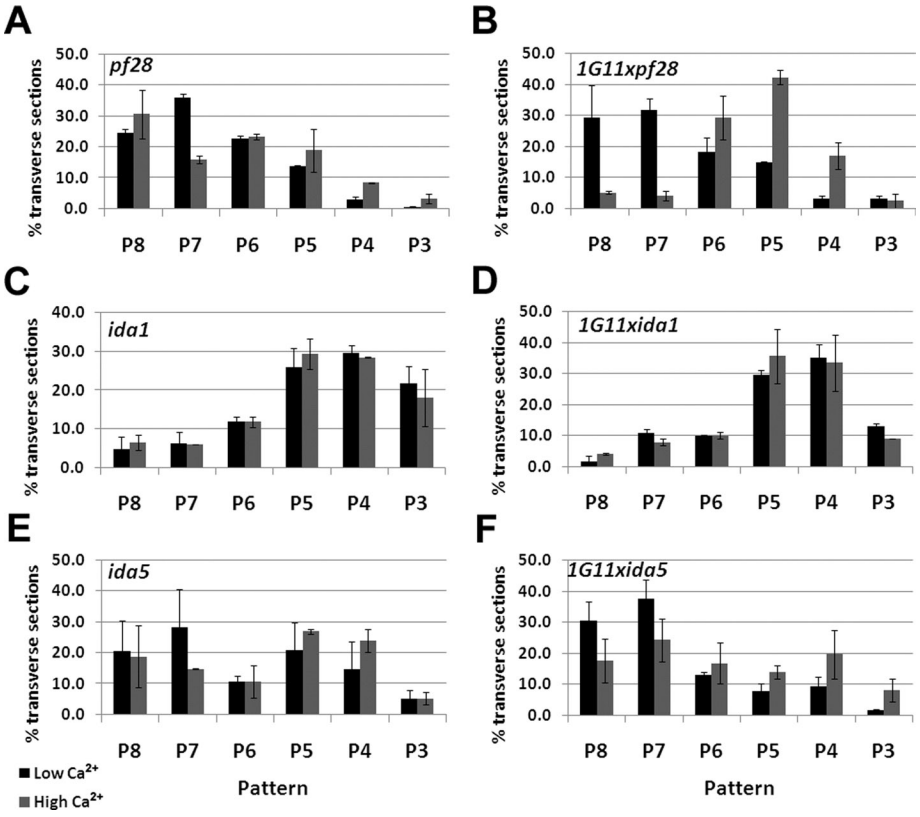

FIGURE 7: Microtubule sliding patterns of dynein double mutants are altered from *1G11*. Distributions of microtubule sliding patterns following microtubule sliding in low calcium (black bars) or high calcium (gray bars) concentration. See Figure 2 for definition of sliding pattern. Data represent the average of two trials. (A) *pf28*, n = 189; *pf28* + Ca, n = 179. (B) *1G11xpf28*, n = 102; *1G11xpf28* + Ca, n = 140. (C) *ida1*, n = 141; *ida1* + Ca, n = 151. (D) *1G11xida1*, n = 159; *1G11xida1* + Ca, n = 179. (E) *ida5*, n = 179; *ida5* + Ca, n = 163. (F) *1G11xida5*, n = 136; *1G11xida5* + Ca, n = 146.

sliding patterns. To test this prediction, we analyzed axonemes in which sliding was induced in vitro by thin-section electron microscopy to determine both the orientation of the central pair and the resulting microtubule sliding patterns. Like WT and *1G11*, the C1 microtubule was significantly oriented toward the area of active microtubule sliding in *1G11xpf28*, *1G11xida1*, and *1G11xida5* in both low- and high-calcium conditions (data not shown).

As mentioned earlier, WT axonemes undergo microtubule sliding in vitro to produce distinct patterns in low- versus high-calcium conditions. Similar to *1G11*, we found that *pf28* does not change sliding patterns regardless of calcium concentration (Figure 7A). In striking contrast, the sliding patterns of *1G11xpf28* axonemes are WT (Figure 7B). In the low-calcium condition, the peak pattern is P7–P8, whereas in the high-calcium condition, the peak is P5. These results support the prediction that the loss of outer dynein arms suppresses paralysis in *1G11* by altering the coordination of microtubule sliding among subsets of doublet microtubules.

Microtubule sliding patterns in *ida1* are predominantly P4 and P5 regardless of calcium concentration (Figure 7C), and *1G11xida1* displays the same patterns (Figure 7D). These results imply that the mechanism of suppression in *1G11xida1* is different from that of *1G11xpf28*. The sliding patterns for *ida5* are distributed among the P8, P7, P5, and P4 orientations in low- and high-calcium conditions (Figure 7E). In contrast, *1G11xida5* slid axonemes display a WT distribution of patterns in the low-calcium condition, with the majority of axonemes sliding with P7 and P8 patterns (Figure 7F). On the other hand, *1G11xida5* axonemes in high-calcium buffers mirror the distribution of *ida5* (Figure 7, E and F). Therefore these results suggest that the ability of *1G11xida5* to coordinate microtubule sliding under low- but not high-calcium levels has been altered.

For single dynein mutants and in combination with *1G11*, we also determined which specific doublet was present on the dynein exposed edge as viewed in transverse section. Although the total number of transverse sections that could be analyzed was low for *pf28* mutants, in all cases the double mutants showed the same distribution as the single dynein mutants; specifically, either doublet 1 or doublet 2 was at the dynein exposed edge (Supplemental Figure S1).

DISCUSSION

A fundamental question in the field of ciliary motility concerns how multiple dynein isoforms are locally regulated to generate complex axonemal bending patterns. In addition, we still do not know how parameters such as waveform and beat frequency are modulated by changes in intracellular second messengers such as calcium. Our previous studies established a role for the Pcdp1 complex associated with the C1d projection of the central apparatus in the regulation of ciliary motility (DiPetrillo and Smith, 2010). The goal of the present work is to elucidate the molecular mechanism of this regulation. Several conclusions can be made from these studies: 1) C1d is not required for generating WT dynein-driven microtubule sliding velocities or for orienting C1 toward the active area of sliding; 2) C1d is required for coordination of dynein activity on specific doublets; and 3) C1d differentially affects the activity of both the outer and inner dynein arms.

The C1d projection/Pcdp1 complex plays a distinct role in flagellar motility

Analyses of *Chlamydomonas* mutants not only demonstrated the importance of the central apparatus in generating wild-type motility, but also revealed that projections associated with each of the two central tubules have distinct functions. For example, mutants lacking the entire central apparatus or the C1 microtubule are paralyzed (Witman *et al.*, 1978; Dutcher *et al.*, 1984; Smith and Lefebvre, 1996), whereas those lacking distinct central apparatus components have altered motility phenotypes. Loss of C1a (*pf6*) leads to twitchy flagella that are inefficient at propelling the cell forward (Dutcher *et al.*, 1984). When the C1b projection fails to assemble (*cpc1*), flagella display a reduced beat frequency (Mitchell and Sale, 1999). Failure of C2b to assemble (hydin RNA interference) results in flagella that pause at the switch points between the effective and recovery strokes (Lechtreck and Witman, 2007), and the loss of C1d (FAP74ami) results in gross motility defects, including a decreased percentage of cells that swim, reduced swimming velocity, reduced beat frequency, and abnormal waveforms (DiPetrillo and Smith, 2010). What we do not know is the molecular mechanism by which specific central pair

projections modulate dynein-driven microtubule sliding to regulate motility. The results presented here provide new insights into the function of the C1d projection.

Previous studies of central pair defective mutants using an in vitro microtubule sliding assay showed that dynein-driven sliding velocities are reduced in mutants lacking the entire central apparatus and the C1 microtubule but not in mutants lacking the C1a or C1b projection (Smith, 2002b). Similarly, we found that sliding velocities in the *1G11* mutant lacking C1d are WT (Figure 1B). Therefore the motility defect in *1G11* is not due to an overall inhibition of dynein activity as seems to be the case in mutants lacking the radial spokes (Smith and Sale, 1992) or entire central apparatus (Smith, 2002b).

C1d is required for coordination of dynein-driven microtubule sliding

Many structural and functional studies using several different model organisms have contributed to a model in which physical interactions between the central pair projections and the radial spokes locally control the direction and extent of axoneme curvature as bends are propagated along the length of the cilium (reviewed in Mitchell, 2009). This model may include a feedback mechanism such that dynein-driven microtubule sliding induces curvature, and curvature, in turn, affects the ability of dynein arms to generate force between specific doublets (e.g., Lindemann and Lesich, 2010; Lindemann, 2011; Woolley, 2010; Wirschell *et al.*, 2011). Presumably the radial spokes and central apparatus provide positional cues about the extent of curvature along the length of the axoneme as waves are propagated. On the basis of the phenotypes of the central apparatus–defective mutants described earlier, interactions of particular central pair projections with the spokes may provide unique regulatory cues controlling specific parameters of bend propagation.

This model also predicts a relationship between central apparatus orientation and active microtubule sliding on specific doublets. On the basis of this logic, mutants lacking specific central pair projections may have defects in central apparatus orientation and/or in coordinating sliding between specific doublet microtubules. It should be noted that the central apparatus rotates in several protists, such as *Chlamydomonas*, but not in cilia and flagella of metazoans (Tamm and Tamm, 1981). However, the central apparatus may still play a role in specifying dynein activity on specific doublets in these organisms. Studies in mussel gill cilia and echinoderm sperm have shown that the central apparatus maintains a specific orientation relative to the position of active sliding (Sale, 1986; Mohri *et al.*, 1987; Satir and Matsuoka, 1989; Holwill and Satir, 1994; Nakano *et al.*, 2003). In these cilia and flagella, the central pair may positively or negatively regulate sliding between doublets by a switching mechanism that includes structural cues other than rotation.

To test the hypothesis that there is a relationship between central pair orientation and active sliding, we previously used an in vitro microtubule sliding assay, followed by transmission electron microscopy (Wargo and Smith, 2003; Wargo *et al.*, 2004). We found that in *pf6* and *cpc1* axonemes the C1 microtubule is oriented toward the area of active sliding, as in WT axonemes. Therefore neither the C1b nor the C1a projections alone are required for maintaining this orientation. Analysis of transverse sections of slid 1G11 axonemes (Figure 2C), revealed that C1d alone is also not required for proper C1 orientation toward the area of active microtubule sliding. By the process of elimination, it follows that C1c or C2 is required for C1 orientation. Alternatively, the presence of any C1 projection may be sufficient to orient the central apparatus. Distinguishing between these possibilities will require the generation of mutants specifically lacking C1c, C2, or different combinations of projections.

The same sliding assay revealed that C1d is required for coordinating dynein activity on specific doublets. On the basis of our previous work (Wargo *et al.*, 2004) combined with that of the Mitchell lab (Mitchell, 2003) using isolated *Chlamydomonas* axonemes, the in vitro sliding assay appears to capture one phase of the beat cycle, the principal bend of the effective stroke. Therefore analyses of sliding patterns may only represent a single snapshot of the beat cycle. Nevertheless, these data reveal important information about the location of active sliding between subsets of doublet microtubules. In addition, the sliding pattern in low- and high-calcium buffers appears to correlate with waveform (Olson and Linck, 1977; Sale, 1986; Nakano *et al.*, 2003).

In low-calcium conditions WT axonemes slide with predominately a P7–P8 pattern, whereas in high-calcium conditions, WT axonemes slide with predominantly a P4–P5 pattern (Wargo *et al.*, 2004). *1G11* axonemes primarily slide with a P5–P6 pattern regardless of calcium condition, indicating that regulatory cues controlling dynein activity on specific doublets are disrupted in the absence of the C1d projection. The disruption of regulatory cues results in active sliding between microtubules at different locations within the axoneme compared with WT. Of interest, sliding patterns are disrupted in the C1a-defective mutant, *pf6*, but not the C1b-defective mutant, *cpc1* (Wargo *et al.*, 2004). Yet the sliding patterns of *pf6* are distinct from those generated from *1G11* axonemes; *pf6* produces P7–P8 patterns regardless of calcium condition. These data provide additional evidence that each central pair projection has a distinct function in controlling ciliary motility.

C1d differentially regulates outer and inner dynein arms

One surprising discovery was that the lack of specific dynein arms suppresses paralysis in the FAP74 amiRNA mutants. This suppression was not strain specific, since the same suppression was observed in two different amiRNA strains (*1G11* and *2D4*) with reduced FAP74 expression. The presence of dynein arm mutations also did not alter the amiRNA-mediated reduction in FAP74 expression; Western blots of double mutants confirmed that FAP74 expression remains significantly reduced in double-mutant strains. Therefore the recovery of motility appears to result from suppression of paralysis caused by the absence of the C1d projection.

Loss of the outer dynein arms in C1d-defective mutants leads to an increased motile population and restores coordination between the two flagella and conversion to a more WT waveform, and yet beat frequency remains unaffected. These results indicate that the beat frequency defect observed in *1G11* is largely due to misregulation of the outer dynein arms. The mechanism by which the inner dynein arms in *1G11xpf28* are differentially regulated to generate an apparently WT waveform without increasing beat frequency is unknown. In general, it is also not known how synchrony between the two flagella is achieved. Given the small population of *1G11* cells that are actually motile, the restoration of synchrony in the double mutant is most likely a function of overall restoration of motility.

Second mutations in outer dynein arms have been previously reported to partially restore motility in paralyzed *Chlamydomonas* mutants lacking either the radial spokes or the central pair (Huang *et al.*, 1982). The *sup-pf1* and *sup-pf2* mutations occur in the outer dynein arm β and γ heavy chains, respectively, and restore motility to spokeless or central pairless flagella without restoring the missing structures (Huang *et al.*, 1982; Porter *et al.*, 1994; Rupp *et al.*, 1996). Importantly, analysis of motility in double mutants with either

mutation combined with a central pairless mutation (*pf15*) revealed that restored motility is not WT. The asymmetric waveform is severely defective due to an increase in symmetry, and beat frequencies are decreased 67–80% compared with WT (Brokaw and Luck, 1985). Although these beat frequencies are similar to those observed for *1G11xpf28*, *1G11xpf28* has nearly fully recovered waveforms that are not seen in either suppressed central pairless mutant *sup-pf1xpf15* or *sup-pf2xpf15*. This difference in suppression is most likely due to the difference in axoneme structures remaining in the two sets of suppressed double mutants. *1G11xpf28* is lacking C1d and the entire row of outer dynein arms. In contrast, *sup-pf1xpf15* and *sup-pf2xpf15* are lacking the entire central apparatus; however, partial outer dynein arms assemble. It should be noted that double mutants with other mutations affecting the central apparatus (*pf6, cpc1*, or *pf18*) and lacking outer dynein arms or specific outer dynein arm motor domains are completely paralyzed (unpublished results; Sakakibara *et al.*, 1993; Porter *et al.*, 1994; Liu *et al.*, 2008). In addition, although bends can be induced to propagate in *pf18*-mutant flagella when external force is applied, no such bends is induced for the mutant *pf18oda1* (Hayashibe *et al.*, 1997). Therefore this extreme suppression, restoring nearly wild-type motility, is specific to mutants lacking the C1d projection.

Similar to *1G11xpf28*, double-mutant analysis of *1G11xida1* revealed an increase in the motile population and restored coordination between the two flagella and conversion to a more WT waveform. However, unlike *1G11xpf28*, *1G11xida1* displays a striking increase in beat frequency. Mutations in inner dynein arm I1 have been reported to suppress paralysis in central pair–defective *Chlamydomonas* mutants. The *pf9-2* mutation was isolated as a suppressor of a temperature-sensitive allele of *pf16* (*pf16BR3*; at the restrictive temperature this strain has defects in C1 stability) and, like *ida1*, results in the failure of I1 to assemble (Porter *et al.*, 1992). When the *pf9-2* mutation is combined with the *pf16BR3* allele, only "weak motility" is restored at the restrictive temperature; further quantification of motility was not described (Porter *et al.*, 1992). The strong recovery of motility in *1G11xida1* is thus distinct from that previously reported for *pf9-2xpf16BR3*. These results provide additional evidence to support the hypothesis that inner dynein arm I1 has an inhibitory function (reviewed in Wirschell *et al.*, 2007). The loss of this inhibition is sufficient to suppress paralysis in flagella lacking the C1d projection, including increasing beat frequency.

Although *1G11xida5* did not increase the percentage of motile cells compared with *1G11*, the motile cells did display a significant increase in beat frequency and swimming velocity. In comparison, mutations in the dynein regulatory complex (DRC) subunits also affect inner dynein arm assembly, and these mutations also suppress paralysis in central pairless *Chlamydomonas* mutants. Inner dynein arms e and b are lacking from *sup-pf3* and *pf2*, whereas the inner dynein arm e alone is lacking from *sup-pf5* and *pf3* (Huang *et al.*, 1982; Piperno *et al.*, 1992, 1994; Gardner *et al.*, 1994; Rupp and Porter, 2003). When these suppressor mutations are combined with a paralyzed central pairless mutant, regular flagellar beating is recovered; however, the movements are insufficient to move the cell forward (Piperno *et al.*, 1994). This difference in recovery level is likely due to the variable components remaining on the axoneme in these mutants. *1G11xida5* lacks C1d and inner dynein arms a and c–e. DRC suppressor mutants in a central pairless background lack the entire central apparatus, various dynein regulatory complex components, and inner dynein arm e alone or in combination with inner dynein arm b, depending on the specific mutant.

Mechanism of regulation

Although previous studies showed that mutants with defects in the central pair or radial spokes can be induced to beat using buffer conditions of varying salts and organic compounds (Yagi and Kamiya, 2000), these structures are required for wild-type motility under physiologic conditions. Our data reveal new insights into control of ciliary motility by the Pcdp1/C1d projection. This complex is required for coordinating dynein activity on specific subsets of doublet microtubules and appears to be involved in regulating motility in both low- and high-calcium conditions. Furthermore, this lack of coordination in C1d-defective mutants is suppressed by mutations in either the outer or inner dynein arm, although the mechanism of suppression appears to differ between these two classes of dynein arm mutants. These results support the hypothesis of Hayashibe *et al.* (1997) that outer and inner dynein arms represent two different motor systems for controlling beating. Our results are also consistent with the results presented by Kikushima (2009) indicating that the central pair may regulate dynein arms on specific subsets of doublet microtubules. Because the C1d projection is not physically associated with the dynein arms, we hypothesize that C1d must transmit regulatory cues to the dynein arms via interactions with the radial spokes and that these cues are distinct from those imparted by other central pair projections. Presumably, interactions with the radial spokes are transmitted to the dynein arms through the intricate network of structural connections observed among the dynein regulatory complex, inner dynein arms, and outer dynein arms (Nicastro *et al.*, 2006; Heuser *et al.*, 2009). Future work will focus on defining specific interactions between C1d subunits and the radial spoke heads, as well as on understanding the molecular events that occur downstream of spoke–central pair interactions to modulate dynein.

MATERIALS AND METHODS

Strains and cell culture

Chlamydomonas reinhardtii strain A54-e18 (nit1-1, ac17, sr1, mt+) has wild-type motility and was obtained from Paul Lefebvre (University of Minnesota, St. Paul, MN). The strains *pf28*, *ida1*, and *ida5* were obtained from the *Chlamydomonas* Genetics Center (University of Minnesota, Minneapolis, MN). FAP74ami transformants *1G11*, *2D4*, *and 7A4* were generated as described previously (DiPetrillo and Smith, 2010). Double mutants *1G11xpf28*, *1G11xida1*, *1G11xida5* were selected from nonparental ditype or tetratype tetrads and confirmed by Western blot (see later discussion). Cells were grown in constant light in Tris-acetate phosphate (TAP) media (Gorman and Levine, 1965).

Gels and blots

Gel electrophoresis and Western blots were performed as previously described (DiPetrillo and Smith, 2010). Serum antibodies were used at a 1:1000 (IC69), 1:5000 (FAP74), and 1:10,000 (IC138 and actin) dilution in TBS-T (Tris buffered saline plus 0.1% Tween 20, as described in DiPetrillo and Smith, 2010). Anti-IC138 serum was generously provided by Winfield Sale (Emory University, Atlanta, GA). Anti-IC69 serum was graciously provided by George Witman (University of Massachusetts Medical Center, Worcester, MA). Monoclonal anti-actin antibodies were purchased from Millipore (Billerica, MA). Polyclonal anti-FAP74 was generated against synthetic peptides based on confirmed cDNA sequence as described previously (DiPetrillo and Smith, 2010).

Analysis of flagellar beat frequency, swimming velocity, and swimming behavior

High-speed video microscopy was performed using a PCO 1200hs camera (Cooke Corporation, Romulus, MI) at 500 fps using phase

contrast optics and a 40× objective on an Axioskope 2 microscope (Zeiss, Thornwood, NY). Images were recorded as 16 bit with a 640 × 480 pixel resolution using PCO.CamWare software (Cooke Corporation). A red filter was used during asymmetric waveform video recordings to prevent photoshock. To induce waveform conversion, the red filter was removed during video recording. Both beat frequency and swimming velocity were measured manually or with ImageJ software (National Institutes of Health, Bethesda, MD), and statistical significance was determined using a Student's *t* test. Beat frequency and swimming velocity data were graphed using Excel (Microsoft, Redmond, WA) and proved to have a normal distribution (data not shown). To determine the percentage of flagellar synchrony, between seven and 14 beats were scored for 32 cells for each strain. The percentage synchrony was calculated by dividing the total number of in-synch beats by the total number of beats scored for each strain.

The ability of strains to photoaccumulate was assessed by covering a Petri dish filled with cells with a black plastic bag and leaving only a small edge exposed to light at an intensity of 9.2 microeinsteins (2.0 W/m^2). An aliquot of cells was taken from the exposed edge of the dish at 0, 5, 15, 30, 60, 120, and 180 min and the cell concentration use calculated by using a hemacytometer. The fold change in concentration over time compared with the 0-min time point was plotted using Excel. Strains *ida5* and *1G11xida5* were "clumpy"; therefore, before any motility assessment, these strains were treated with autolysin to remove mother cell walls and then shaken in TAP media for 1 h to ensure that cells had full-grown flagella.

Calculating the radius of curvature

High-speed videos of each cell strain swimming with the asymmetric waveform were analyzed in ImageJ. The video was stopped when the flagellum of interest was in the mid recovery stroke. With the ImageJ circle tool, a circle was drawn to fit the curvature of the principal bend of the recovery stroke. The diameter was measured using the measure tool calibrated to a stage micrometer. The diameter was divided in half to calculate the radius. Ten radii were calculated for each cell strain, and the average is graphed in Supplemental Figure S2. Excel was used to calculate the SD and the Student's *t* test p values for each strain set; WT was compared to *1G11*, *ida1* to *1G11xida1*, *ida5* to *1G11xida5*, and *pf28* to *1G11xpf28*.

Axoneme isolation, microtubule sliding, and electron microscopy

Flagella were severed from cell bodies by the dibucaine method (Witman, 1986) and isolated by differential centrifugation in buffer A (10 mM 4-(2-hydroxyethyl)-1-piperazineethanesulfonic acid, pH 7.4, 5 mM $MgSO_4$, 1 mM dithiothreitol, 0.5 mM EDTA, and 50 mM potassium acetate). Axonemes were isolated by adding NP-40 (Calbiochem, La Jolla, CA) to flagella for a final concentration of 0.5% (wt/vol) to remove flagellar membranes. Measurement of sliding velocity between doublet microtubules was based on the methods of Okagaki and Kamiya (1986). Microtubule sliding was initiated with buffer A containing 1 mM ATP and 2 μg/ml type VIII protease (Sigma-Aldrich, St. Louis, MO) and was recorded as described previously (Smith, 2002a). Distance of sliding was measured using ImageJ software, and velocity was calculated as a function of change in time. All data are presented as mean ± SEM. The Student's *t* test was used to determine the significance of differences between means. For experiments done in the presence of high Ca^{2+} (pCa 4), buffer A was modified to contain 1.7 mM $CaCl_2$, 0.1 mM ethylene glycol tetraacetic acid, and 2.0 mM EDTA (Wakabayashi *et al.*, 1997).

For some experiments, exactly 3 min after the addition of sliding buffer (buffer A containing 1 mM ATP and 4 μg/ml type VIII protease), 8% glutaraldehyde was added to the sample for a final concentration of 1%, and the sample was pelleted and processed for electron microscopy. Specimens were fixed with 1% glutaraldehyde and 1% tannic acid in 0.1 M sodium cacodylate, postfixed in 1% osmium tetroxide, dehydrated in a graded series of ethanol, and embedded in LX112 resin (LADD Research, Williston, PA). Uniform silver-gray sections were mounted on copper/palladium grids (EMS, Hatfield, PA), stained with uranyl acetate and Reynolds lead citrate, and examined at 100 kV in a transmission electron microscope model (JEM-1010; JEOL, Tokyo, Japan) with side-mounted 2K × 2K AMT (Advanced Microscopy Techniques, Woburn, MA) camera.

Statistical analysis of images

Transverse sections of axonemes lacking doublet microtubules were considered axonemes in which microtubule sliding was induced after the addition of ATP and protease. For each experiment, every transverse section in which sliding occurred and the C1 and C2 microtubules could be distinguished was analyzed for central apparatus orientation. All images were oriented with the dynein arms projecting clockwise, the axoneme viewed proximal to distal. Axoneme transverse sections corresponded to one of six different sliding patterns (Figure 2A). For each pattern, the axoneme was partitioned into active and inactive areas. The active area is the position in which microtubule sliding resulted in the loss of doublets from the remainder of the axoneme; this area included the exposed A-tubule and dynein arms and extended to the exposed B-tubule. The inactive area is the remainder of the axoneme.

To determine whether the correlation between the orientation of the central apparatus and the position of active microtubule sliding was significant, we used the total number of events for each pattern to calculate how many times we expected to observe the C1 microtubule oriented toward the active area if central apparatus orientation was random. For the example provided in Figure 2A, there were a total of 29 slid axonemes observed in the P8 orientation (13 were active and 16 were inactive). To determine the expected distribution, we calculated that 2/9 of the circumference of the axoneme constitutes the active area, whereas the remaining 7/9 constitutes the inactive area. On the basis of these fractions, if the orientation of the central apparatus were completely random, then the C1 microtubule would have a 2/9 chance for pointing toward the active area and a 7/9 chance of pointing at the inactive area. Therefore, since we had a total of 29 slid axonemes in the P8 orientation, C1 would be expected to orient toward the active area of sliding in 6.44 transverse sections (29 × 2/9) and toward the inactive area in 22.56 images (29 × 7/9). This calculation was made for each pattern of microtubule sliding, then summed for all patterns, and finally expressed as a percentage of the total number of transverse sections included in the analysis. In the example provided in Figure 2A, if the orientation of the central pair were random, we would expect to find C1 oriented toward the active area of sliding in 42.45% of all transverse section images. What we actually observed was that C1 was oriented toward the active area in 72.65% of the transverse sections. We used the χ^2 test to determine significance of differences between the number of observed and expected events. Probability values were calculated using the CHIDIST function in Excel. For each strain and condition, our results represent data collected from two independent experiments.

ACKNOWLEDGMENTS

We thank Louisa Howard (Dartmouth College, Hanover, NH) for technical assistance with electron microscopy. This work was supported by National Institutes of Health Grant GM66919 (E.F.S.), Training Grant 2-T32-GM008704 (C.G.D.), and Copenhaver/Thomas Fellowship (C.G.D.).

REFERENCES

Bessen M, Fay RB, Witman GB (1980). Calcium control of waveform in isolated flagellar axonemes of *Chlamydomonas*. J Cell Biol 86, 446–455.

Brokaw CJ, Luck DJ (1985). Bending patterns of *Chlamydomonas* flagella: III. A radial spoke head deficient mutant and a central pair deficient mutant. Cell Motil 5, 195–208.

DiPetrillo CG, Smith EF (2010). Pcdp1 is a central apparatus protein that binds Ca(2+)-calmodulin and regulates ciliary motility. J Cell Biol 189, 601–612.

Dutcher SK, Huang B, Luck DJ (1984). Genetic dissection of the central pair microtubules of the flagella of *Chlamydomonas reinhardtii*. J Cell Biol 98, 229–236.

Dymek EE, Smith EF (2007). A conserved CaM- and radial spoke associated complex mediates regulation of flagellar dynein activity. J Cell Biol 179, 515–526.

Gardner LC, O'Toole E, Perrone CA, Giddings T, Porter ME (1994). Components of a "dynein regulatory complex" are located at the junction between the radial spokes and the dynein arms in *Chlamydomonas flagella*. J Cell Biol 127, 1311–1325.

Gorman DS, Levine RP (1965). Cytochrome f and plastocyanin: their sequence in the photosynthetic electron transport chain of *Chlamydomonas reinhardtii*. Proc Natl Acad Sci USA 54, 1665–1669.

Habermacher G, Sale WS (1997). Regulation of flagellar dynein by phosphorylation of a 138-kD inner arm dynein intermediate chain. J Cell Biol 136, 167–176.

Hayashibe K, Shingyoji C, Kamiya R (1997). Induction of temporary beating in paralyzed flagella of *Chlamydomonas* mutants by application of external force. Cell Motil Cytoskeleton 37, 232–239.

Hendrickson TW, Perrone CA, Griffin P, Wuichet K, Mueller J, Yang P, Porter ME, Sale WS (2004). IC138 is a WD-repeat dynein intermediate chain required for light chain assembly and regulation of flagellar bending. Mol Biol Cell 15, 5431–5442.

Heuser T, Raytchev M, Krell J, Porter ME, Nicastro D (2009). The dynein regulatory complex is the nexin link and a major regulatory node in cilia and flagella. J Cell Biol 187, 921–933.

Holwill ME, Satir P (1994). Physical model of axonemal splitting. Cell Motil Cytoskeleton 27, 287–298.

Hoops HJ, Witman GB (1983). Outer doublet heterogeneity reveals structural polarity related to beat direction in *Chlamydomonas* flagella. J Cell Biol 97, 902–908.

Horst CJ, Witman GB (1993). ptx1, a nonphototactic mutant of *Chlamydomonas*, lacks control of flagellar dominance. J Cell Biol 120, 733–741.

Huang B, Ramanis Z, Luck DJ (1982). Suppressor mutations in *Chlamydomonas* reveal a regulatory mechanism for flagellar function. Cell 28, 115–124.

Hyams JS, Borisy GG (1978). Isolated flagellar apparatus of *Chlamydomonas*: characterization of forward swimming and alteration of waveform and reversal of motion by calcium ions in vitro. J Cell Sci 33, 235–253.

Kamiya R (1988). Mutations at twelve independent loci result in absence of outer dynein arms in *Chlamydomonas reinhardtii*. J Cell Biol 107, 2253–2258.

Kamiya R, Kurimoto E, Muto E (1991). Two types of *Chlamydomonas* flagellar mutants missing different components of inner-arm dynein. J Cell Biol 112, 441–447.

Kamiya R, Witman GB (1984). Submicromolar levels of calcium control the balance of beating between the two flagella in demembranated models of *Chlamydomonas*. J Cell Biol 98, 97–107.

Kato T, Kagami O, Yagi T, Kamiya R (1993). Isolation of two species of *Chlamydomonas reinhardtii* flagellar mutants, ida5 and ida6, that lack a newly identified heavy chain of the inner dynein arm. Cell Struct Funct 18, 371–377.

Kato-Minoura T, Hirono M, Kamiya R (1997). *Chlamydomonas* inner-arm dynein mutant, ida5, has a mutation in an actin-encoding gene. J Cell Biol 137, 649–656.

Kikushima K (2009). Central pair apparatus enhances outer-arm dynein activities through regulation of inner-arm dyneins. Cell Motil Cytoskeleton 66, 272–280.

King SJ, Dutcher SK (1997). Phosphoregulation of an inner dynein arm complex in *Chlamydomonas reinhardtii* is altered in phototactic mutant strains. J Cell Biol 136, 177–191.

King SM, Kamiya R (2009). Witman GB (2009). Axonemal dyneins: assembly, structure, and force generation. The *Chlamydomonas* Sourcebook, Vol. 3. Cell Motility and Behavior, New York: Elsevier, 131–191.

Lechtreck KF, Witman GB (2007). *Chlamydomonas reinhardtii* hydin is a central pair protein required for flagellar motility. J Cell Biol 176, 473–482.

Lee L, Campagna DR, Pinkus JL, Mulhern H, Wyatt TA, Sisson JH, Pavlik JA, Pinkus GS, Fleming MD (2008). Primary ciliary dyskinesia in mice lacking the novel ciliary protein Pcdp1. Mol Cell Biol 28, 949–957.

Lindemann CB (2011). Experimental evidence for the geometric clutch hypothesis. Curr Top Dev Biol 95, 1–31.

Lindemann CB, Lesich KA (2010). Flagellar and ciliary beating: the proven and the possible. J Cell Sci 123, 519–528.

Liu Z, Takazaki H, Nakazawa Y, Sakato M, Yagi T, Yasunaga T, King SM, Kamiya R (2008). Partially functional outer-arm dynein in a novel *Chlamydomonas* mutant expressing a truncated gamma heavy chain. Eukaryot Cell 7, 1136–1145.

Mitchell DR (2003). Orientation of the central pair complex during flagellar bend formation in Chlamydomonas. Cell Motil Cytsokeleton 56, 120–129.

Mitchell DR (2009). The flagellar central pair apparatus. In: The *Chlamydomonas* Sourcebook, Vol. 3. Cell Motility and Behavior, ed. GB Witman, New York: Elsevier, 235–248.

Mitchell DR, Kang Y (1991). Identification of oda6 as a *Chlamydomonas* dynein mutant by rescue with the wild-type gene. J Cell Biol 113, 835–842.

Mitchell DR, Rosenbaum JL (1985). A motile *Chlamydomonas* flagellar mutant that lacks outer dynein arms. J Cell Biol 100, 1228–1234.

Mitchell DR, Sale WS (1999). Characterization of a *Chlamydomonas* insertional mutant that disrupts flagellar central pair microtubule-associated structures. J Cell Biol 144, 293–304.

Mohri H, Mohri T, Okuno M (1987). Topographical relationship between the axonemal arrangement and the bend direction in starfish sperm flagella. Cell Motil Cytoskeleton 8, 76–84.

Myster SH, Knott JA, O'Toole E, Porter ME (1997). The *Chlamydomonas* Dhc1 gene encodes a dynein heavy chain subunit required for assembly of the I1 inner arm complex. Mol Biol Cell 8, 607–620.

Nakano I, Kobayashi T, Yoshimura M, Shingyoji C (2003). Central-pair-linked regulation of microtubule sliding by calcium in flagellar axonemes. J Cell Sci 116, 1627–1636.

Nicastro D, Schwartz C, Pierson J, Gaudette R, Porter ME, McIntosh JR (2006). The molecular architecture of axonemes revealed by cryoelectron tomography. Science 313, 944–948.

Okagaki T, Kamiya R (1986). Microtubule sliding in mutant *Chlamydomonas* axonemes devoid of outer or inner dynein arms. J Cell Biol 103, 1895–1902.

Okita N, Isogai N, Hirono M, Kamiya R, Yoshimura K (2005). Phototactic activity in *Chlamydomonas* 'non-phototactic' mutants deficient in Ca2+-dependent control of flagellar dominance or in inner-arm dynein. J Cell Sci 118, 529–537.

Olson GE, Linck RW (1977). Observations of the structural components of flagellar axonemes and central pair microtubules from rat sperm. J Ultrastruct Res 61, 21–43.

Omoto CK, Gibbons IR, Kamiya R, Shingyoji C, Takahashi K, Witman GB (1999). Rotation of the central pair microtubules in eukaryotic flagella. Mol Biol Cell 10, 1–4.

Patel-King RS, Benashski SE, King SM (2002). A bipartite Ca2+-regulated nucleoside-diphosphate kinase system within the *Chlamydomonas* flagellum. The regulatory subunit p72. J Biol Chem 277, 34271–34279.

Patel-King RS, Gorbatyuk O, Takebe S, King SM (2004). Flagellar radial spokes contain a Ca2+-stimulated nucleoside diphosphate kinase. Mol Biol Cell 15, 3891–3902.

Piperno G, Luck DJ (1979). An actin-like protein is a component of axonemes from *Chlamydomonas* flagella. J Biol Chem 254, 2187–2190.

Piperno G, Mead K, LeDizet M, Moscatelli A (1994). Mutations in the "dynein regulatory complex" alter the ATP-insensitive binding sites for inner arm dyneins in *Chlamydomonas* axonemes. J Cell Biol 125, 1109–1117.

Piperno G, Mead K, Shestak W (1992). The inner dynein arms I2 interact with a "dynein regulatory complex" in *Chlamydomonas* flagella. J Cell Biol 118, 1455–1463.

Porter ME, Knott JA, Gardner LC, Mitchell DR, Dutcher SK (1994). Mutations in the SUP-PF-1 locus of *Chlamydomonas reinhardtii* identify a regulatory domain in the beta-dynein heavy chain. J Cell Biol 126, 1495–1507.

Porter ME, Power J, Dutcher SK (1992). Extragenic suppressors of paralyzed flagellar mutations in *Chlamydomonas reinhardtii* identify loci that alter the inner dynein arms. J Cell Biol 118, 1163–1176.
Ruffer U, Nultsch W (1998). Flagellar coordination in *Chlamydomonas* cells held on micropipettes. Cell Motil Cytoskeleton 41, 297–307.
Rupp G, O'Toole E, Gardner LC, Mitchell BF, Porter ME (1996). The sup-pf-2 mutations of *Chlamydomonas* alter the activity of the outer dynein arms by modification of the gamma-dynein heavy chain. J Cell Biol 135, 1853–1865.
Rupp G, Porter ME (2003). A subunit of the dynein regulatory complex in *Chlamydomonas* is a homologue of a growth arrest-specific gene product. J Cell Biol 162, 47–57.
Sakakibara H, Takada S, King SM, Witman GB, Kamiya R (1993). A *Chlamydomonas* outer arm dynein mutant with a truncated beta heavy chain. J Cell Biol 122, 653–661.
Salathe M (2007). Regulation of mammalian ciliary beating. Annu Rev Physiol 69, 401–422.
Sale WS (1986). The axonemal axis and Ca2+-induced asymmetry of active microtubule sliding in sea urchin sperm tails. J Cell Biol 102, 2042–2052.
Satir P (1968). Studies on cilia. 3. Further studies on the cilium tip and a "sliding filament" model of ciliary motility. J Cell Biol 39, 77–94.
Satir P (1985). Switching Mechanisms in the Control of Ciliary Motility, New York: Alan R. Liss.
Satir P, Matsuoka T (1989). Splitting the ciliary axoneme: implications for a "switch-point" model of dynein arm activity in ciliary motion. Cell Motil Cytoskeleton 14, 345–358.
Smith EF (2002a). Regulation of flagellar dynein by calcium and a role for an axonemal calmodulin and calmodulin-dependent kinase. Mol Biol Cell 13, 3303–3313.
Smith EF (2002b). Regulation of flagellar dynein by the axonemal central apparatus. Cell Motil Cytoskeleton 52, 33–42.
Smith EF, Lefebvre PA (1996). PF16 encodes a protein with armadillo repeats and localizes to a single microtubule of the central apparatus in *Chlamydomonas* flagella. J Cell Biol 132, 359–370.
Smith EF, Sale WS (1991). Microtubule binding and translocation by inner dynein arm subtype I1. Cell Motil Cytoskeleton 18, 258–268.
Smith EF, Sale WS (1992). Regulation of dynein-driven microtubule sliding by the radial spokes in flagella. Science 257, 1557–1559.
Smith EF, Yang P (2004). The radial spokes and central apparatus: mechano-chemical transducers that regulate flagellar motility. Cell Motil Cytoskeleton 57, 8–17.
Summers KE, Gibbons IR (1971). Adenosine triphosphate-induced sliding of tubules in trypsin-treated flagella of sea-urchin sperm. Proc Natl Acad Sci USA 68, 3092–3096.
Summers KE, Gibbons IR (1973). Effects of trypsin digestion on flagellar structures and their relationship to motility. J Cell Biol 58, 618–629.
Tamm SL, Tamm S (1981). Ciliary reversal without rotation of axonemal structures in ctenophore comb plates. J Cell Biol 89, 495–509.
Tash JS, Krinks M, Patel J, Means RL, Klee CB, Means AR (1988). Identification, characterization, and functional correlation of calmodulin-dependent protein phosphatase in sperm. J Cell Biol 106, 1625–1633.
Wakabayashi K, Yagi T, Kamiya R (1997). Ca2+-dependent waveform conversion in the flagellar axoneme of *Chlamydomonas* mutants lacking the central-pair/radial spoke system. Cell Motil Cytoskeleton 38, 22–28.
Wargo MJ, Dymek EE, Smith EF (2005). Calmodulin and PF6 are components of a complex that localizes to the C1 microtubule of the flagellar central apparatus. J Cell Sci 118, 4655–4665.
Wargo MJ, McPeek MA, Smith EF (2004). Analysis of microtubule sliding patterns in *Chlamydomonas* flagellar axonemes reveals dynein activity on specific doublet microtubules. J Cell Sci 117, 2533–2544.
Wargo MJ, Smith EF (2003). Asymmetry of the central apparatus defines the location of active microtubule sliding in *Chlamydomonas* flagella. Proc Natl Acad Sci USA 100, 137–142.
Wilkerson CG, King SM, Witman GB (1994). Molecular analysis of the gamma heavy chain of *Chlamydomonas* flagellar outer-arm dynein. J Cell Sci 107 (Pt 3), 497–506.
Wirschell M, Hendrickson T, Sale WS (2007). Keeping an eye on I1: I1 dynein as a model for flagellar dynein assembly and regulation. Cell Motil Cytoskeleton 64, 569–579.
Wirschell M, Nicastro D, Porter ME, Sale WS (2009). The regulation of axonemal bending. In: The *Chlamydomonas* Sourcebook, Vol. 3. Cell Motility and Behavior, ed. GB Witman, New York: Elsevier, 253–282.
Wirschell M, Yamamoto R, Alford L, Gokhale A, Gaillard A, Sale WS (2011). Regulation of ciliary motility: conserved protein kinases and phosphatases are targeted and anchored in the ciliary axoneme. Arch Biochem Biophys 510, 93–100.
Witman GB (1986). Isolation of *Chlamydomonas* flagella and flagellar axonemes. Methods Enzymol 134, 280–290.
Witman GB (1993). *Chlamydomonas* phototaxis. Trends Cell Biol 3, 403–408.
Witman GB, Plummer J, Sander G (1978). *Chlamydomonas* flagellar mutants lacking radial spokes and central tubules. Structure, composition, and function of specific axonemal components. J Cell Biol 76, 729–747.
Woolley DM (2010). Flagellar oscillation: a commentary on proposed mechanisms. Biol Rev Camb Philos Soc 85, 453–470.
Yagi T, Kamiya R (2000). Vigorous beating of *Chlamydomonas* axonemes lacking central pair/radial spoke structures in the presence of salts and organic compounds. Cell Motil Cytoskeleton 46, 190–199.
Yang P, Diener DR, Rosenbaum JL, Sale WS (2001). Localization of calmodulin and dynein light chain LC8 in flagellar radial spokes. J Cell Biol 153, 1315–1326.
Yang P, Smith EF (2009). The flagellar radial spokes. In: The *Chlamydomonas* Sourcebook, Vol. 3. Cell Motility and Behavior, 2nd ed., ed. GB Witman, New York: Elsevier, 209–234.
Yoshimura M, Shingyoji C (1999). Effects of the central pair apparatus on microtubule sliding velocity in sea urchin sperm flagella. Cell Struct Funct 24, 43–54.